

(Supporting information)

Ligand Exchange on Au₃₈(SR)₂₄: Substituent Site Effects of Aromatic Thiols

Yingwei Li^a, Rosalba Juarez-Mosqueda^b, Yongbo Song^c, Yuzhuo Zhang^a, Jinsong Chai^a,
Giannis Mpourmpakis^{*b}, and Rongchao Jin^{*a}

^aDepartment of Chemistry, Carnegie Mellon University, Pittsburgh, Pennsylvania 15213, United States

^bDepartment of Chemical Engineering, University of Pittsburgh, Pittsburgh, Pennsylvania 15261, United States

^cDepartment of Chemistry and Centre for Atomic Engineering of Advanced Materials, Anhui Province Key Laboratory of Chemistry for Inorganic/Organic Hybrid Functionalized Materials, Anhui University, Hefei, Anhui 230601, People's Republic of China.

*Email: (R.J.) rongchao@andrew.cmu.edu; (G.M.) GMPOURMP@pitt.edu

Chemicals

Tetrachloroauric (III) acid (HAuCl₄·3H₂O, 99.999% metal basis, Aldrich), sodium borohydride (NaBH₄, 99.99% metal basis, Aldrich), glutathione (HSG, 98%, Acros Organics), 2-phenylethanethiol (PET, 99%, Aldrich), 2-methylbenzenethiol (2MBT, 97% Acros Organics), 1-naphthalenethiol (1SNap, 99%, Alfa Aesar), 2,4-dimethylbenzenethiol (2,4DMBT, 95%, Aldrich), 2-ethylbenzenethiol (2EBT, 95%, TCI America), 2,5-dimethylbenzenethiol (2,5DMBT, 97%, Aldrich), 2,6-dimethylbenzenethiol (2,6DMBT, 97%, Alfa Aesar), 2-methyl-5-*tert*-butylbenzenethiol (5TB2MBT, 90%, TCI America), 2-fluorobenzenethiol (2FBT, 97%, Aldrich), 2-methoxybenzenethiol (2MOBT, 97%, Aldrich), 2-naphthalenethiol (2SNap, 98%, Alfa Aesar), 4-methylbenzenethiol (4MBT, 98%, Aldrich), 3,4-dimethylbenzenethiol (3,4DMBT, 98%, Aldrich), 4-ethylbenzenethiol (4EBT, 97%, TCI America), 4-*tert*-butyl-benzenethiol (TBBT, 97%, Alfa Aesar), 4-fluorobenzenethiol (4FBT, 98%, Aldrich), 4-methoxybenzenethiol (4MOBT, 97%, Aldrich), 3-methylbenzenethiol (3MBT, 95%, Aldrich) and 3,5-dimethylbenzenethiol (3,5DMBT, 97%, TCI America), benzenethiol (SPh, 97%, Aldrich), cyclopentanethiol (CPT, 97%, Aldrich), cyclohexanethiol (CHT, 97%, Aldrich), acetone (HPLC grade, 99.9%, Aldrich), toluene (HPLC grade, 99.9%, Aldrich), ethanol (HPLC grade, Aldrich), methanol (HPLC grade, 99.9%, Aldrich), and dichloromethane (DCM, HPLC grade, 99.9%, Aldrich), were used as received.

Characterization of Nanoclusters

UV-vis spectra of the clusters were measured on a Hewlett-Packard Agilent 8453 diode array spectrophotometer at room temperature. For the cryo measurements, the 2-methyltetrahydrofuran solutions of clusters were used to form clear glass at 80 K, followed by UV-vis measurements on a Shimadzu UV-3600 plus spectrometer. MALDI mass spectrometry (MALDI-MS) was performed on a PerSeptive Biosystems Voyager DE super-STR time-of-flight (TOF) mass spectrometer.

X-ray Crystallographic Determination of Au₃₈(2,4DMBT)₂₄.

Single crystal X-ray diffraction data of Au₃₈(2,4DMBT)₂₄ was collected on a Bruker APEX-II CCD diffractometer. The crystal was kept at 296.15 K during data collection. Using Olex2,¹ the structure

was solved with the ShelXT² structure solution program using Intrinsic Phasing and refined with the ShelXL³ refinement package using Least Squares minimization. Crystal Data for $C_{32}H_{36}Au_{6.333333}S_4$ ($M=1796.30$ g/mol): trigonal, space group R-3c (no. 167), $a = 19.522(6)$ Å, $c = 129.34(4)$ Å, $V = 42689(29)$ Å³, $Z = 36$, $T = 296.15$ K, $\mu(\text{MoK}\alpha) = 19.707$ mm⁻¹, $D_{\text{calc}} = 2.515$ g/cm³, 106588 reflections measured ($1.89^\circ \leq 2\theta \leq 54.8^\circ$), 10415 unique ($R_{\text{int}} = 0.1489$, $R_{\text{sigma}} = 0.0879$) which were used in all calculations. The final R_1 was 0.0637 ($I > 2\sigma(I)$) and wR_2 was 0.1873 (all data).

TDDFT computational methods

Structure optimizations and photoabsorption spectrum calculations were carried out for the $Au_{38}(\text{DMBT})_{24}$ and $Au_{38}(\text{PET})_{24}$ nanoclusters within the framework of density functional theory (DFT) and time-dependent DFT using the PBE functional.⁴ All the calculations were performed using a real-space grid with spacing of 0.2 Å in GPAW.^{5,6} The crystal structure of $Au_{38}(\text{PET})_{24}$ and $Au_{38}(\text{DMBT})_{24}$ were obtained from the experimental X-ray structure determination. The atomic charges were analyzed based on the Bader method.⁷ The symmetry of the structures was determined by using the symmetry tool of VMD with a tolerance criterion of 0.02.

SI Figures:

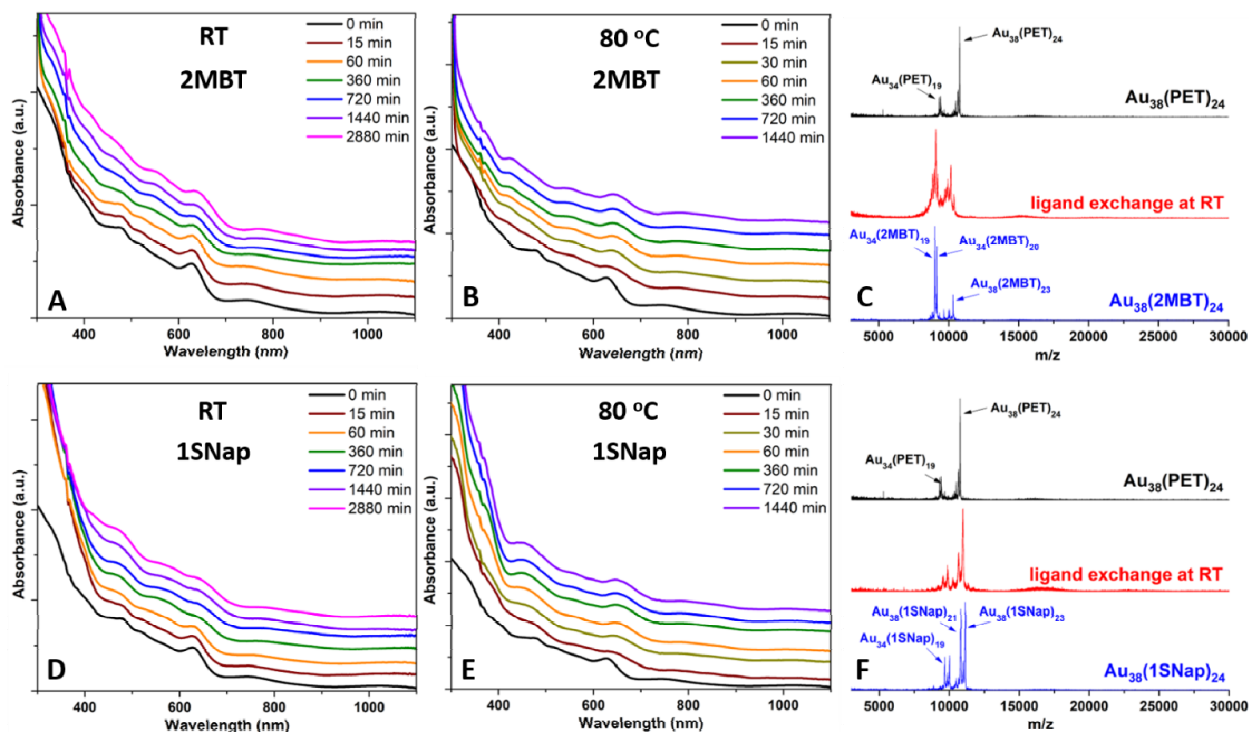


Figure S1. Time-dependent UV-vis spectra of ligand exchange on $Au_{38}(\text{PET})_{24}$ with 2MBT at (A) RT, (B) 80 °C, and (C) their corresponding MALDI-MS spectra; or by 1SNap at (D) RT, (E) 80 °C, and (F) their corresponding MALDI-MS spectra.

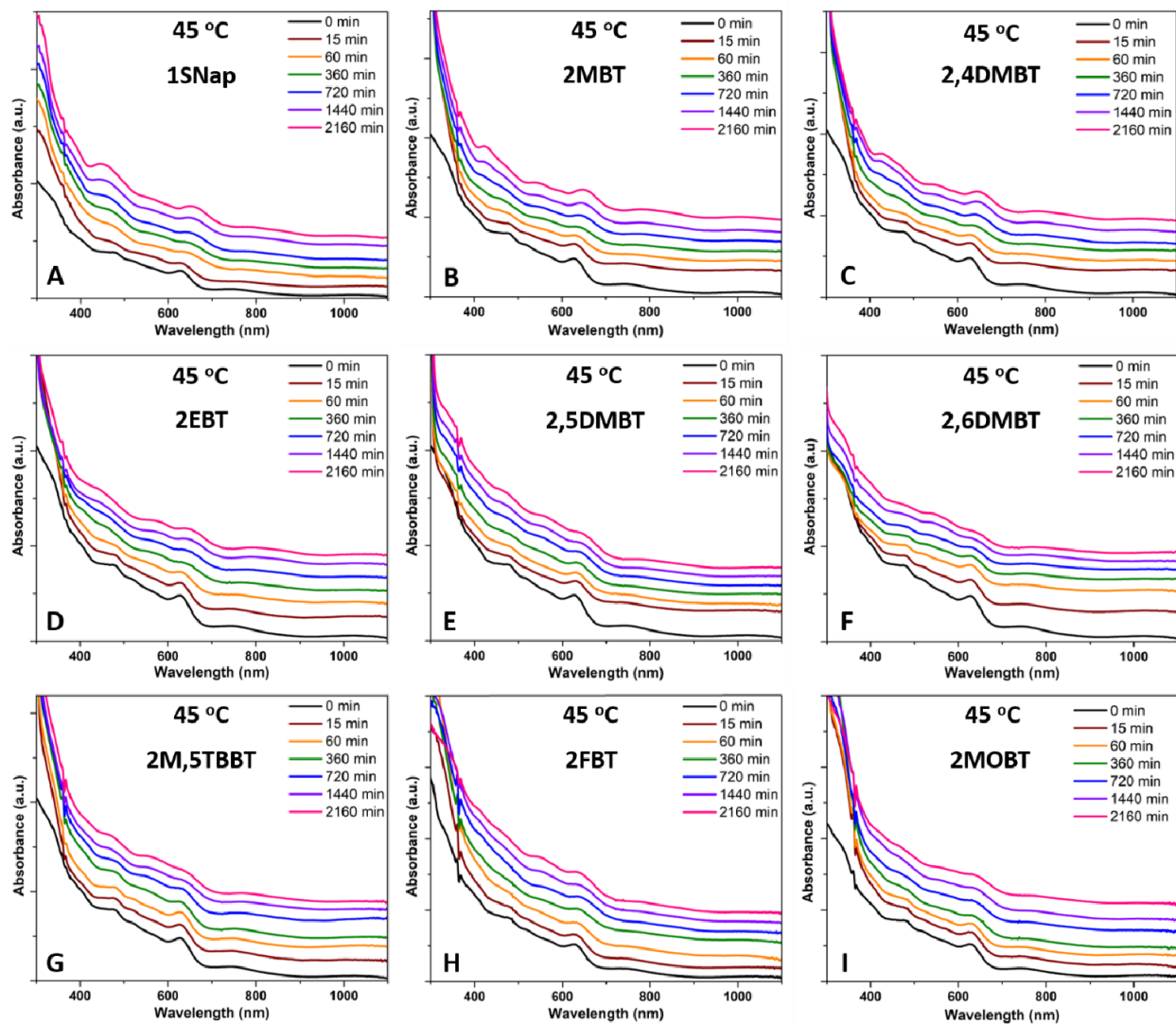


Figure S2. Time-dependent UV-vis spectra of ligand exchange on $\text{Au}_{38}(\text{PET})_{24}$ with (A) 1SNap; (B) 2MBT; (C) 2,4DMBT; (D) 2EBT; (E) 2,5DMBT; (F) 2,6DMBT; (G) 2M,5TBBT; (H) 2FBT; and (I) 2MOBT at 45 °C.

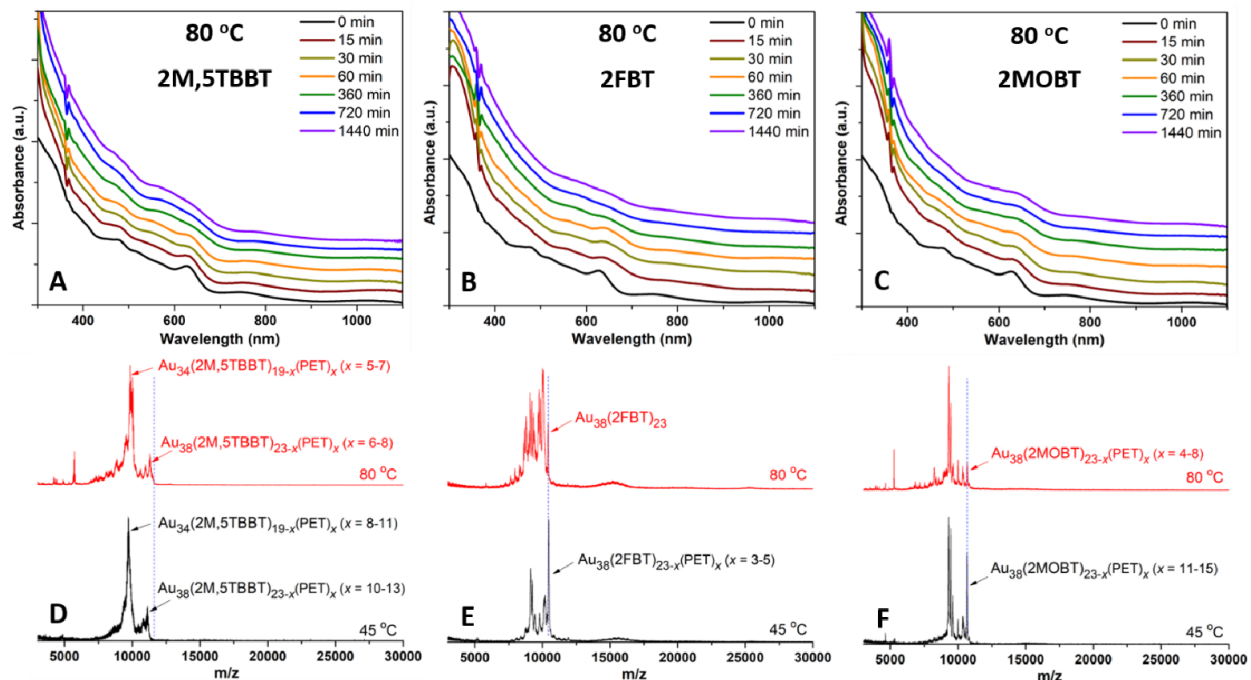


Figure S3. Time-dependent UV-vis spectra of ligand exchange on $\text{Au}_{38}(\text{PET})_{24}$ with (A) 2M,5TBBT; (B) 2FBT; and (C) 2MOBT at 80 °C. (D/E/F) Corresponding MALDI-MS spectra of the samples prepared at 80 °C or 45 °C. Dashed lines indicate the m/z of fully ligand-exchanged Au_{38} .

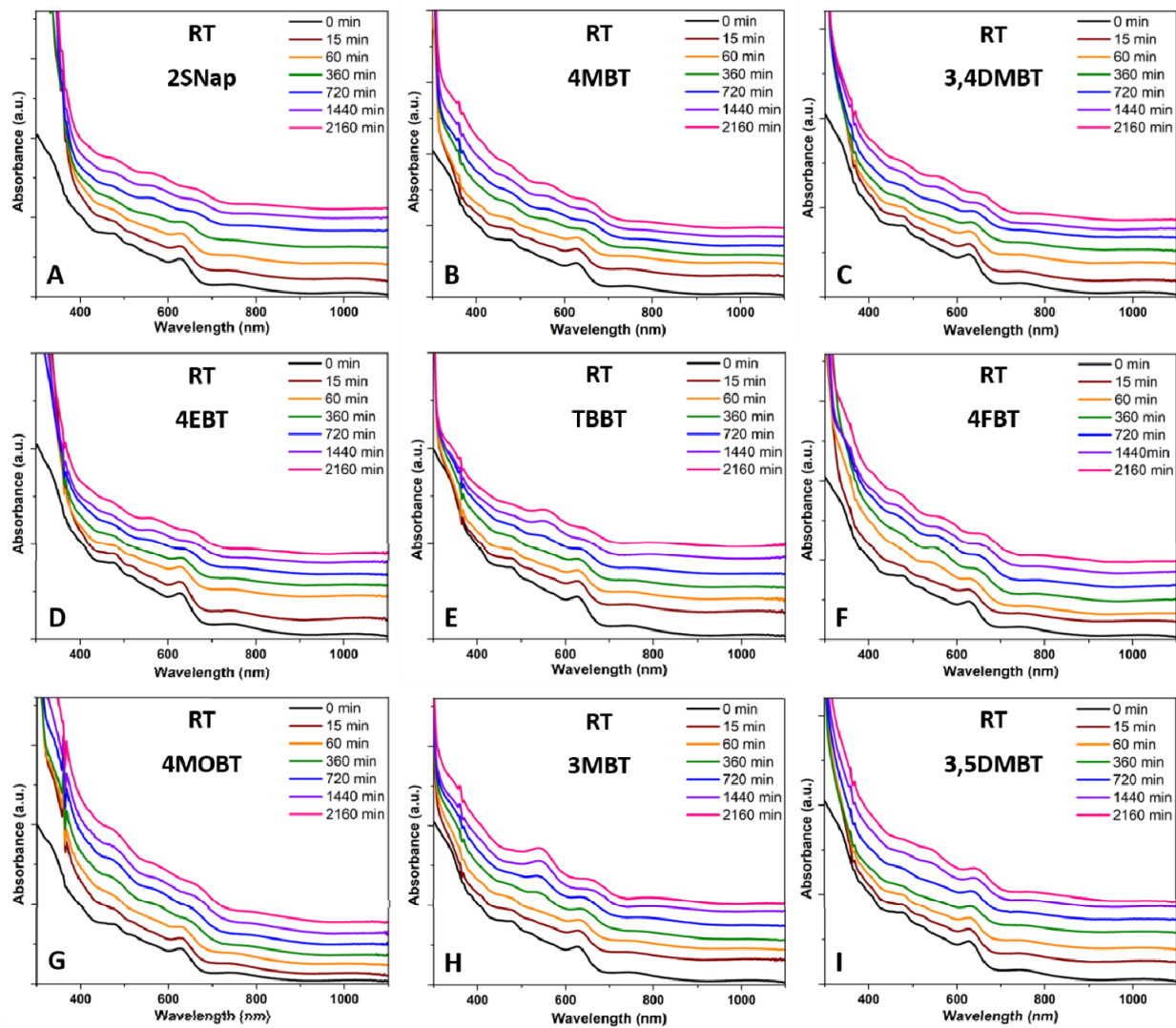


Figure S4. Time-dependent UV-vis spectra of ligand exchange on $\text{Au}_{38}(\text{PET})_{24}$ with (A) 2SNap; (B) 4MBT; (C) 3,4DMBT; (D) 4EBT; (E) TBBT; (F) 4FBT; (G) 4MOBT; (H) 3MBT; and (I) 3,5DMBT at RT.

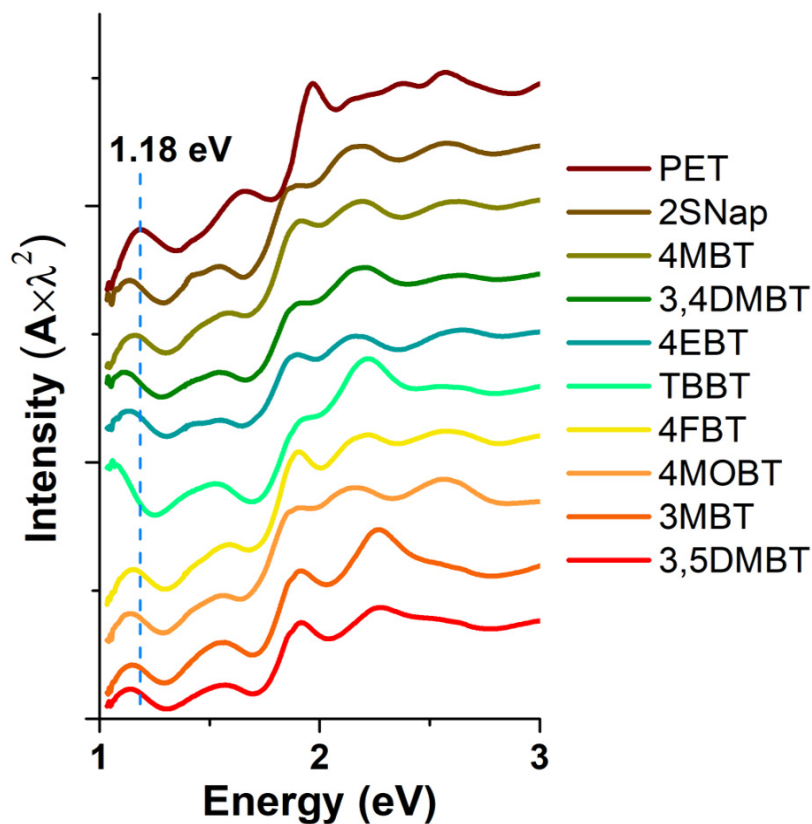


Figure S5. UV-vis-NIR spectra (RT) of different $\text{Au}_{38}(\text{SR})_{24}$ NCs. Dashed lines indicate the lowest-energy absorption peak position of $\text{Au}_{38}(\text{PET})_{24}$.

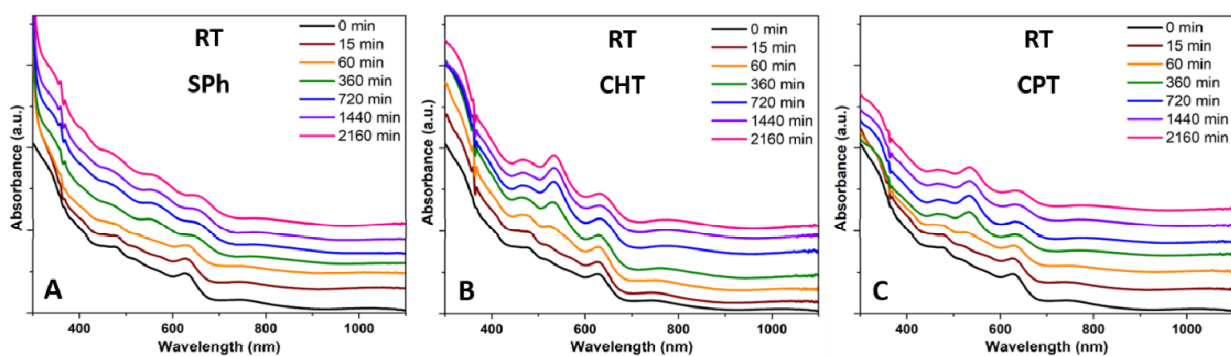


Figure S6. Time-dependent UV-vis spectra of ligand exchange on $\text{Au}_{38}(\text{PET})_{24}$ with (A) SPH; (B) CHT; and (C) CPT at RT.

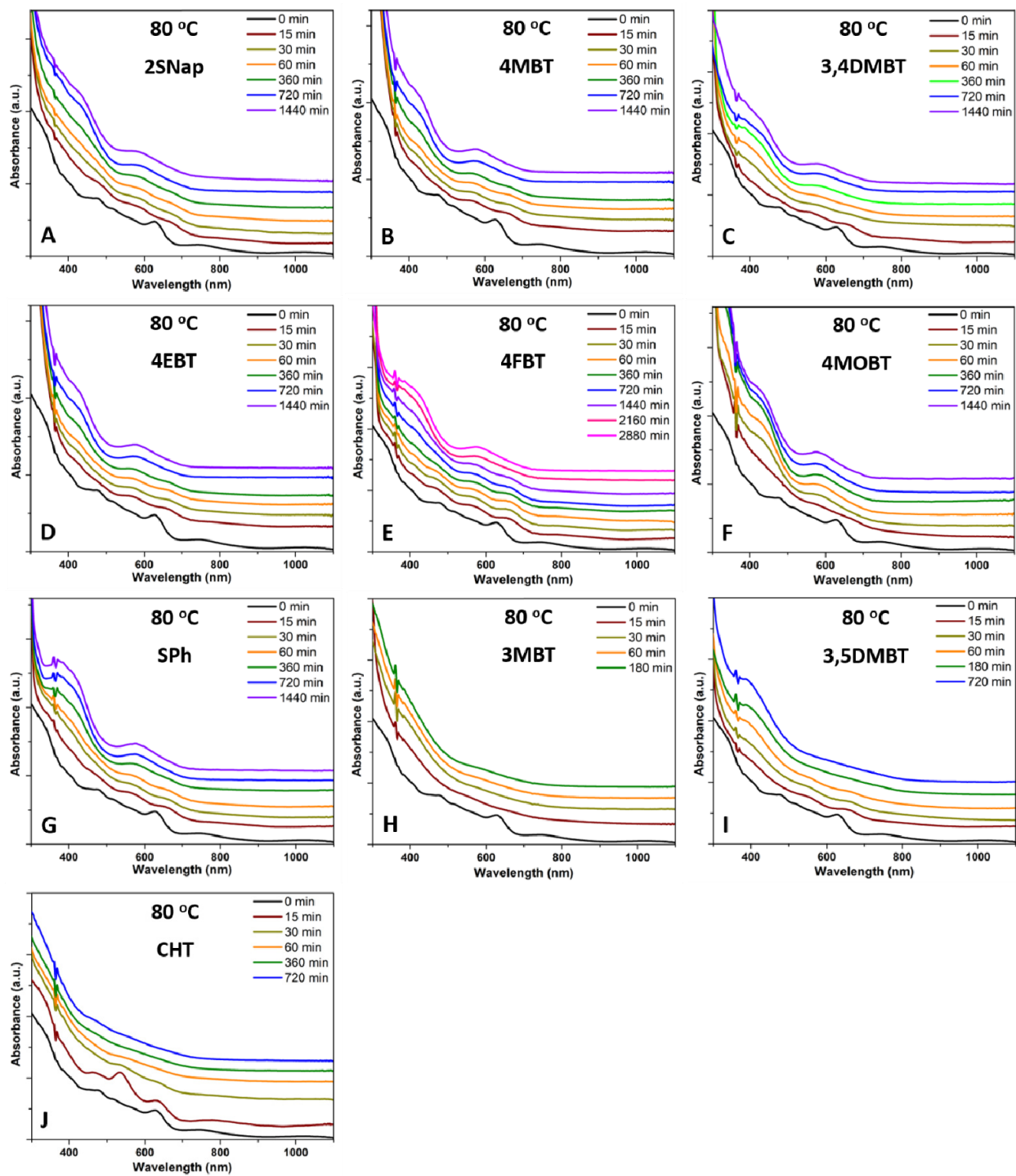


Figure S7. Time-dependent UV-vis spectra of ligand exchange on $\text{Au}_{38}(\text{PET})_{24}$ with (A) 2SNap; (B) 4MBT; (C) 3,4DMBT; (D) 4EBT; (E) 4FBT; (F) 4MOBT; (G) SPh; (H) 3MBT; (I) 3,5DMBT; and (J) CHT at 80 °C.

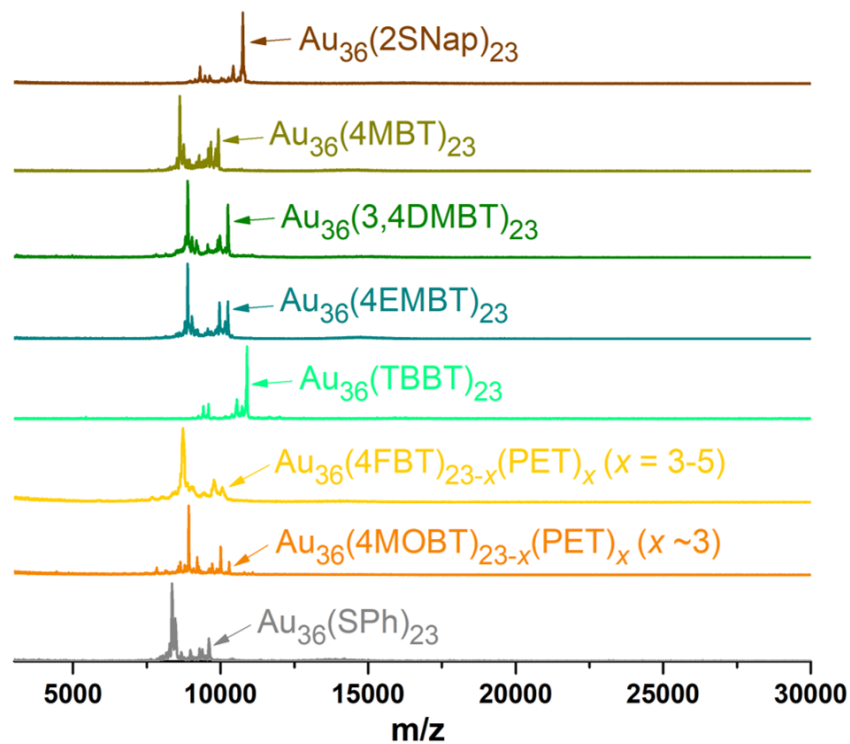


Figure S8. MALDI-MS spectra for different $\text{Au}_{36}(\text{SR})_{24}$.

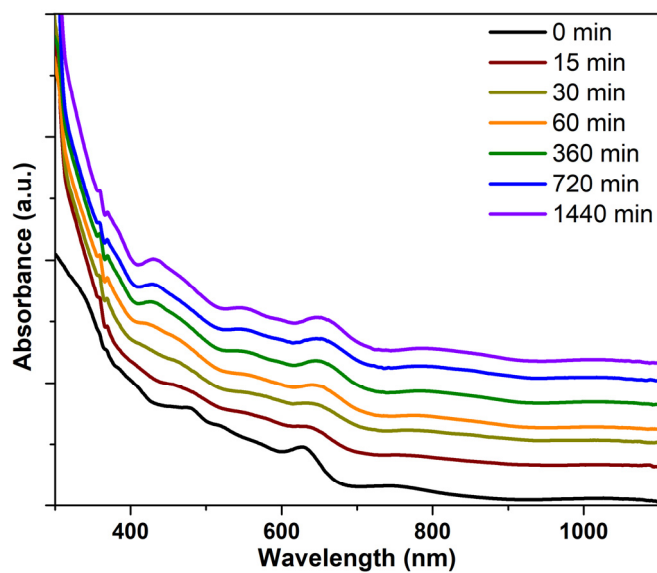


Figure S9. Time-dependent UV-vis spectra of ligand exchange on $\text{Au}_{38}(\text{PET})_{24}$ with 2,4DMBT at $80\text{ }^{\circ}\text{C}$.

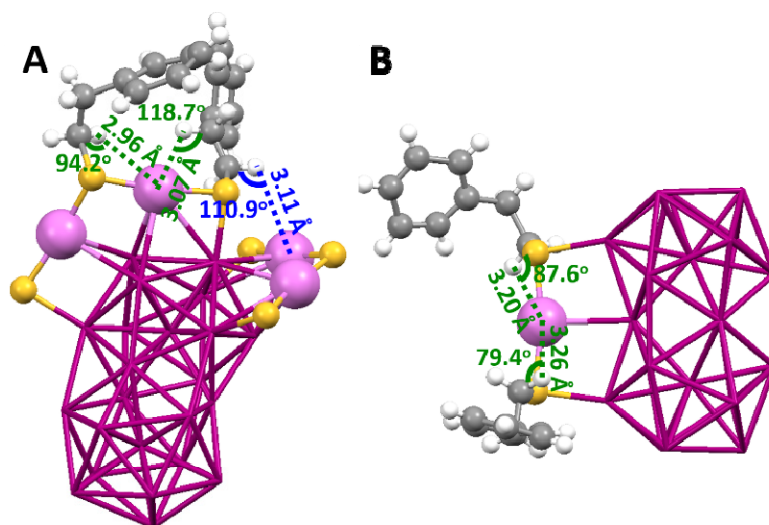


Figure S10. The shortest distances between Au and H from (A) the dimeric $\text{Au}_2(\text{PET})_3$ motif ligands; (B) the monomeric $\text{Au}(\text{PET})_2$ motif ligands, and their corresponding $\angle\text{Au-H-C}$ angles.

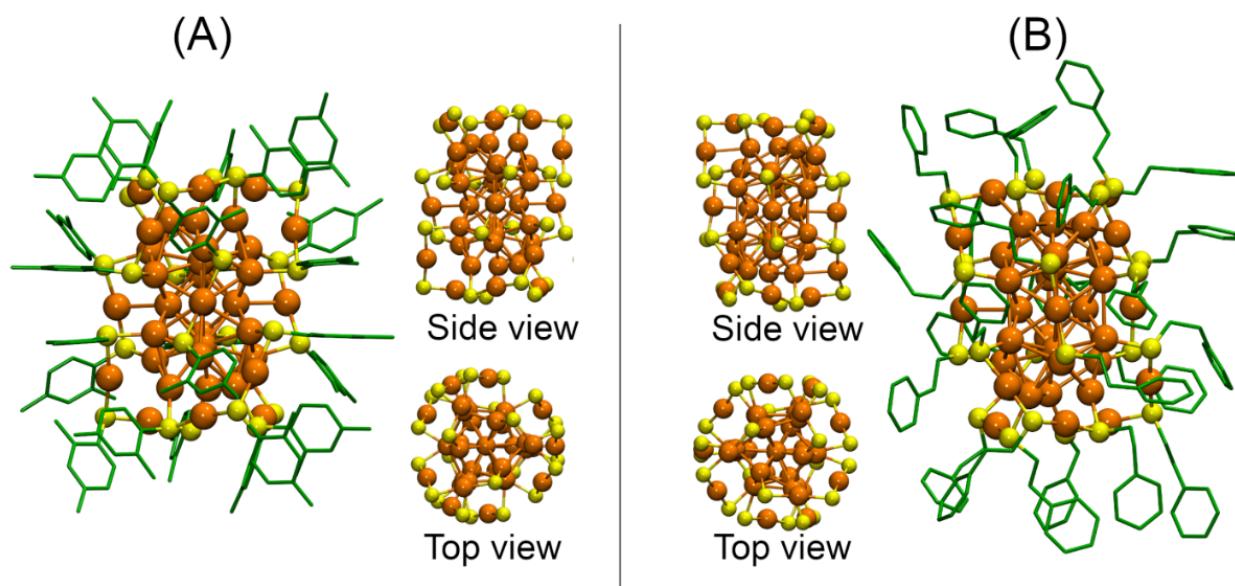


Figure S11. Optimized structures of (A) $\text{Au}_{38}(\text{2,4DMBT})_{24}$ of D_3 symmetry, and (B) $\text{Au}_{38}(\text{PET})_{24}$ of C_1 symmetry under tolerance values < 0.07 . $\text{Au}_{38}(\text{2,4DMBT})_{24}$ and $\text{Au}_{38}(\text{PET})_{24}$ are shown in different enantiomers.

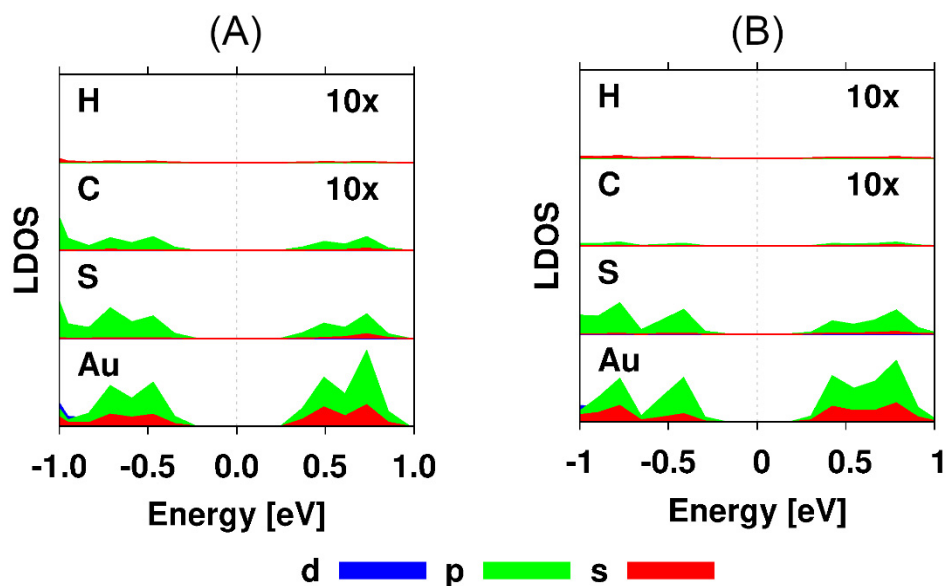


Figure S12. Local projected density of states (LPDOS) per atom type of (A) $\text{Au}_{38}(\text{2,4DMBT})_{24}$ and (B) $\text{Au}_{38}(\text{PET})_{24}$ nanoclusters. Fermi energy of $\text{Au}_{38}(\text{2,4DMBT})_{24}$ and $\text{Au}_{38}(\text{PET})_{24}$ is -3.696 eV and -3.822 eV, respectively. The s, p and d refer to atomic orbitals.

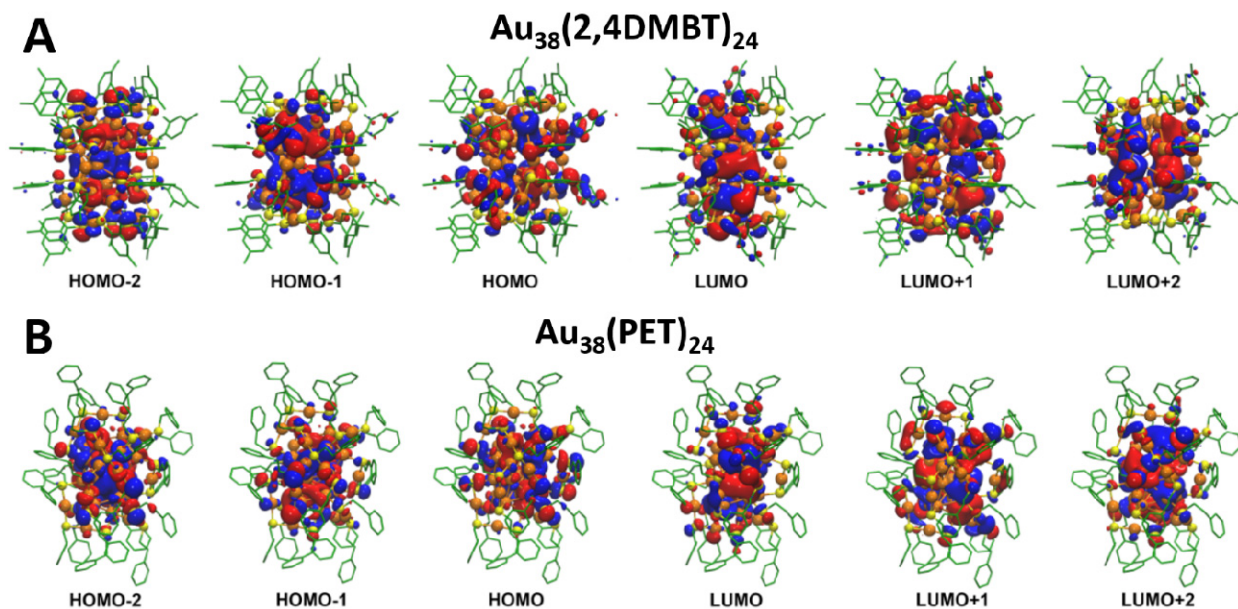


Figure S13. Kohn-Sham orbital diagrams of (A) $\text{Au}_{38}(\text{2,4DMBT})_{24}$ and (B) $\text{Au}_{38}(\text{PET})_{24}$ nanoclusters.

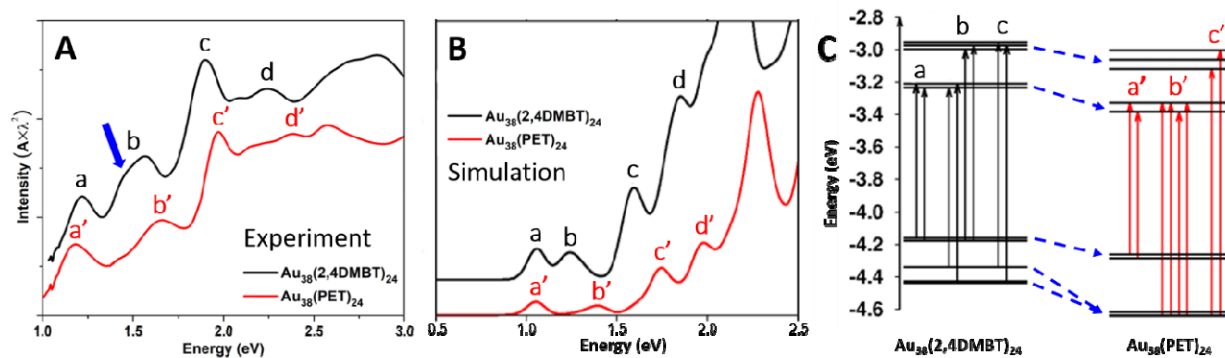


Figure S14. (A) Experimental, (B) simulated absorption spectra of $\text{Au}_{38}(\text{2,4DMBT})_{24}$ and $\text{Au}_{38}(\text{PET})_{24}$ NCs, and (C) corresponding Kohn-Sham energy diagrams of frontier molecular orbitals.

Table S1. Electronic transitions contributing to the main absorption peaks **a**, **b**, **c**, **d**, and **a'**, **b'**, **c'** and **d'** of the spectra of the $\text{Au}_{38}(\text{2,4DMBT})_{24}$ and $\text{Au}_{38}(\text{PET})_{24}$ NCs, respectively.

Peak	$\text{Au}_{38}(\text{2,4DMBT})_{24}$	Peak	$\text{Au}_{38}(\text{PET})_{24}$
a	HOMO→LUMO+1	a'	HOMO→LUMO+1
	HOMO-1→LUMO		HOMO-1→LUMO
b	HOMO-2→LUMO	b'	HOMO-4→LUMO+1
	HOMO-4→LUMO+1		HOMO-3→LUMO+1
	HOMO-1→LUMO+2		HOMO-3→LUMO
	HOMO-1→LUMO+3		HOMO-1→LUMO+3
	HOMO→LUMO+3		HOMO-2→LUMO
c	HOMO-3→LUMO	c'	HOMO-3→LUMO+2
	HOMO-5→LUMO+1		HOMO-4→LUMO+4
	HOMO-8→LUMO+1		HOMO-5→LUMO
	HOMO-6→LUMO		HOMO-3→LUMO+3
	HOMO-4→LUMO+3		HOMO-6→LUMO+1
	HOMO-5→LUMO+1		
d	HOMO-2→LUMO+4	d'	HOMO-7→LUMO+2
	HOMO-3→LUMO+3		HOMO-12→LUMO
	HOMO-14→LUMO+1		HOMO-12→LUMO+1
	HOMO-6→LUMO+4		HOMO-6→LUMO+4
	HOMO-7→LUMO+2		HOMO-13→LUMO+1
	HOMO-13→LUMO		
	HOMO-7→LUMO+4		
	HOMO-19→LUMO		

Table S2. Energy of the frontier molecular orbitals of the $\text{Au}_{38}(\text{2,4DMBT})_{24}$ and $\text{Au}_{38}(\text{PET})_{24}$ NCs. States of similar energies are marked by the same color for differentiation.

	$\text{Au}_{38}(\text{2,4DMBT})_{24}$	$\text{Au}_{38}(\text{PET})_{24}$
Molecular Orbital	Energy (eV)	Energy (eV)
HOMO-4	-4.438	-4.642
HOMO-3	-4.427	-4.636
HOMO-2	-4.340	-4.616
HOMO-1	-4.178	-4.285
HOMO	-4.160	-4.261
LUMO	-3.232	-3.383
LUMO+1	-3.211	-3.329
LUMO+2	-2.997	-3.119
LUMO+3	-2.973	-3.062
LUMO+4	-2.956	-3.004

Table S3. Bader charges of $\text{Au}_{38}(\text{2,4DMBT})_{24}$ and $\text{Au}_{38}(\text{PET})_{24}$ nanoclusters calculated per atom type. The charges are calculated for the 23 kernel Au atoms ($\text{Au}_{\text{kernel}}$), the 15 staple Au atoms ($\text{Au}_{\text{staples}}$), the 24 S, 192 C, and 216 H atoms.

	$\text{Au}_{38}(\text{2,4DMBT})_{24}$	$\text{Au}_{38}(\text{PET})_{24}$
$\text{Au}_{\text{kernel}}$	0.043 ± 0.036 (0.982)	0.035 ± 0.031 (0.810)
$\text{Au}_{\text{staples}}$	0.121 ± 0.006 (1.818)	0.102 ± 0.012 (1.528)
S	-0.096 ± 0.020 (-2.297)	-0.154 ± 0.020 (-3.706)
C	-0.066 ± 0.064 (-12.597)	-0.065 ± 0.050 (-12.541)
H	0.056 ± 0.027 (12.077)	0.064 ± 0.025 (13.935)

Reference

1. Dolomanov, O.V., Bourhis, L.J., Gildea, R.J, Howard, J.A.K. & Puschmann, H. *J. Appl. Cryst.* 2009, **42**, 339-341.
2. Sheldrick, G.M. *Acta Cryst.* 2015, A71, 3-8.
3. Sheldrick, G.M. *Acta Cryst.* 2015, C71, 3-8.
4. Perdew, J. P., Burke, K. & Ernzerhof, M. *Physical Review Letters* 1996, **77**, 3865-3868.
5. Mortensen, J. J., Hansen, L. B. & Jacobsen, K. W. *Physical Review B* 2005, **71**, 035109.
6. Enkovaara, J. *et al. Journal of Physics: Condensed Matter* 2010, **22**, 253202.
7. Henkelman, G., Arnaldsson, A. & Jónsson, H. *Computational Materials Science* 2006, **36**, 354-360.